Applied Energy 98 (2012) 562–573

Contents lists available at SciVerse ScienceDirect

Applied Energy

journal homepage: www.elsevier.com/locate/apenergy

A new design method for Organic Rankine Cycles with constraint of inlet and outlet heat carrier fluid temperatures coupling with the heat source

Qicheng Chen [a], Jinliang Xu [b,*], Hongxia Chen [c]

[a] State Key Laboratory of Alternate Electrical Power System with Renewable Energy Sources, North China Electric Power University, Beijing 102206, PR China
[b] The Beijing Key Laboratory of New and Renewable Energy, North China Electric Power University, Beijing 102206, PR China
[c] The Beijing Key Laboratory of Multiphase Flow and Heat Transfer, North China Electric Power University, Beijing 102206, PR China

HIGHLIGHTS

- A new design method for Organic Rankine Cycle was proposed.
- The method directly relates the thermal efficiency with the turbine power output.
- The higher turbine inlet temperatures reduce the turbine inlet pressures to decrease the system thermal efficiency.
- The optimal running condition appears at the saturated or slightly-superheated vapor state at the turbine inlet.
- The exergy destructions by each component of the ORC were identified.

ARTICLE INFO

Article history:
Received 29 January 2012
Received in revised form 17 April 2012
Accepted 21 April 2012
Available online 22 May 2012

Keywords:
Low grade energy
Organic Rankine Cycle
Thermal efficiency
Exergy destruction

ABSTRACT

A design method for ORCs is newly proposed to fully couple the ORC with the heat source. The heat source is characterized by the mass flow rate, inlet and outlet heat carrier fluid temperatures. Example cases were performed to study the optimal running parameters for ORCs with constraint of given heat source and pinch temperature difference in evaporators. Benzene is selected as the working fluid. The results show that a higher turbine inlet temperature requires a lower turbine inlet pressure, leading to a lower system thermal efficiency. The optimal (maximum) thermal efficiency appears at the saturated or slightly-superheated vapor state at the turbine inlet. The pinch temperature differences in evaporators strongly influence the system thermal efficiency. At higher turbine inlet temperatures, either the condenser or the evaporator contributes the major exergy destruction, depending on the flue gas inlet temperatures. At lower turbine inlet temperatures, the evaporator, expander and condenser are the first, second and third contributions of the exergy destruction to the whole system. The exergy destruction by the condenser is significantly decreased with decreases in the turbine inlet temperatures.

1. Introduction

Low grade thermal energy (heat) such as waste heat, geothermal, and heat from low to moderate temperature solar collectors, accounts for more than one half of the total heat generated worldwide [1–4]. A large amount of waste heat is directly released to the environment by industries. It is shown that the aluminum smelters in Canada produce 80 PJ of waste heat annually. If only 10% of this energy was recovered to produce useful work, Canadian aluminum producers could save up to 96 millions dollars per year, and reduce the green house gas emissions by about 0.45 megatons per year [5]. This is only one example illustrating the importance of recovering industrial waste heat. Great progresses have been made to recover the waste heat and produce useful work, allowing industries to become more energy efficient and to improve their productivity. For the past 20 years, extensive researches have been performed on the Organic Rankine Cycle (ORC) for the main purpose of converting low temperature heat (80 °C < T < 300 °C) into electricity [6–10].

Studies on the ORC can be summarized into the following sorts: (1) Modify the basic ORC to have higher thermal efficiency. For instance, including an internal heat exchange (IHE) in the cycle can improve the thermal efficiency [11–13]. (2) Select suitable working fluids for high (~300 °C) and moderate temperature (below 200 °C) heat sources [14–23]. Most working fluids do not work well over a wide temperature range (300–100 °C) of the heat source. (3) Replace subcritical Rankine cycles with supercritical Rankine cycles to have better thermal performance [24–26]. (4) Replace pure working fluids with zeotropic mixture working fluids to have

* Corresponding author. Tel./fax: +86 10 61772268.
E-mail address: xjl@ncepu.edu.cn (J. Xu).

0306-2619/$ - see front matter © 2012 Elsevier Ltd. All rights reserved.
http://dx.doi.org/10.1016/j.apenergy.2012.04.035

Nomenclature

C_p	specific heat (kJ/kg K)
e	specific exergy (kJ/kg)
E	exergy (kW)
h	specific enthalpy (kJ/kg)
I	exergy destruction (kW)
m	mass flow rate (kg/s)
P	pressure (MPa)
Q	heating power (kW)
s	specific entropy (kJ/kg K)
T	temperature (K)
W	power (kW)

Greek symbols

α	the angle for the line CD with respect to the horizontal axis Q in Fig. 2
Δ	difference of quantities or triangle
η	efficiency

Subscripts

1–7	points corresponding to Fig. 1
a	absorb heat for Q_a or available
con	condenser
ex	exergy
eva	evaporator
exp	expander
f	organic fluid
gas	flue gas
i	component
in	inlet
out	outlet
ORC	Organic Rankine Cycle
p	pinch point or pump
s	isentropic
sat	saturation
sys	ORC system
t	turbine or expander
u	used

better thermal performance [27–31]. (5) Search optimal conditions for ORCs [24,32–37].

Bianchi and Pascale [9] noted that among small size bottoming cycle technologies, the identified solutions which could allow to improve the energy saving performance of an existing plant by generating a certain amount of electric energy are: the Organic Rankine Cycle, the Stirling engine and the Inverted Brayton Cycle. The authors provided a parametric investigation of the thermodynamic performance of different systems. A comparison with other existing energy recovery solutions was performed to assess the market potential, showing the highest electric efficiency values of more than 20% with reference to the input heat content with the ORC.

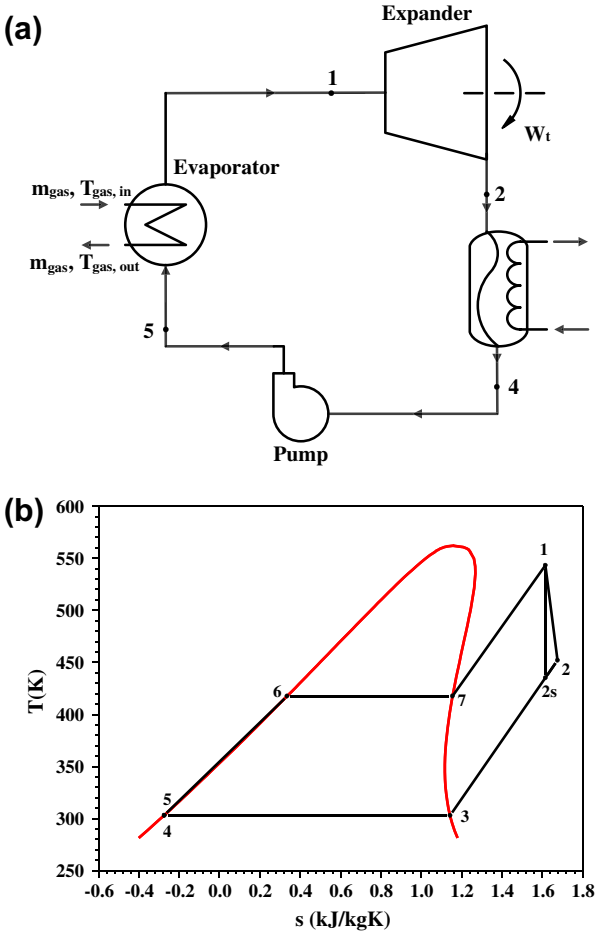

Fig. 1. The basic ORC and a typical T–s diagram.

Roy et al. [22] presented an analysis of non-regenerative ORC based on the parametric optimization using R12, R123, R134a and R717 as working fluids superheated at constant pressure. A computer program was developed to optimize and compare the system and second law efficiency, irreversibility of the system, availability ratio, work output, mass flow rate with increase in turbine inlet temperature under different heat source temperatures. It is found that R123 produces the maximum efficiencies and turbine power with minimum irreversibility for employed constant as well as variable heat source temperatures. Hence, R123 may be the better choice of the working fluid for converting low-grade heat to power.

Wang et al. [23] experimentally studied the performance of a low-temperature solar recuperative ORC using working fluid of R245fa. The experimental setup consisted of throttling valves, liquid pumps, air cooled condensers and a flat plate collector to gather solar energy. The introduction of a recuperator did not improve the thermal efficiency obviously (remaining constant of about 3.67%) at constant fluid flow rates. Preheating caused the increase of the collector inlet temperature, lowering the collector efficiencies and overall system efficiencies. Both the thermal and collector efficiencies could be improved significantly by adjusting the working fluid flow rate to an appropriate value based on the solar heat flux.

Wang et al. [31] presented an experimental study of a low-temperature solar Rankine cycle system for power generation. The cycle performances of pure R245fa and zeotropic mixtures of R245fa/R152a (0.9/0.1) and R245fa/R152a (0.7/0.3) were compared using the experimental prototype. The collector efficiency and thermal efficiency of zeotropic mixtures are higher than pure fluid of R245fa, indicating the potential of using zeotropic mixtures for overall efficiency improvement.

Zhang et al. [24] performed an investigation on the parameter optimization and performance comparison of the fluids in

subcritical ORC and transcritical power cycle in low-temperature (i.e. 80–100 °C) binary geothermal power system. The choice of working fluid varies the objective function and optimized operation parameters are not all the same for different indicators. R123 in subcritical ORC system yields the highest thermal efficiency and exergy efficiency of 11.1% and 54.1%, respectively. It is concluded that R125 in transcritical power cycle shows excellent economic and environmental performance and can maximize utilization of the geothermal, which is preferable for the low-temperature geothermal ORC system. R41 also exhibits favorable performance except for its flammability.

Quoilin et al. [36] described the behavior of a small-scale ORC to recover energy from a variable flow rate and temperature waste heat source. A dynamic model of the ORC was proposed focusing on the control strategy for part-load, start up and shutdown of the ORC system. Three different control strategies were proposed and compared. They show that the predictive model based on the steady state optimization under various conditions shows the best results.

Li et al. [37] presented low temperature solar thermal electric generation system, consisting of compound parabolic concentrators (CPCs) and Organic Rankine Cycle (ORC) working with HCFC-123. A novel design was proposed to reduce heat transfer irreversibility between conduction oil and HCFC-123 in heat exchangers. Three factors have major impact on the annual electricity output and should be the key points of optimization: (1) The annual received direct irradiance can be significantly increased by two or three times optimal adjustments. (2) Two-stage collectors connected with the heat exchangers by two thermal oil cycles can improve the collector efficiency by 8.1–20.9% in the simultaneous processes of heat collection and power generation. (3) On the use of the available market collectors the optimal ORC evaporation temperatures are around 120 °C.

For an ORC with a pure working fluid, the organic fluid shall have the states of subcooled liquid, saturated liquid, saturated vapor consecutively by the continuous heating. Evaporation takes place at a saturation temperature in the two-phase region. Further heating yields the superheated vapor at the outlet. Due to the isothermal boiling of the organic working fluid in evaporators, there is a poor match between the heat carrier fluid of the heat source and the organic working fluid. This is the reason why many people are searching supercritical Rankine cycle, or the cycle with binary working fluids, to improve the thermal match between the heat carrier fluid and the organic working fluid.

Even though many authors noted that the pinch temperature difference in evaporators is important for the ORC, the ORC is analyzed without complete coupling with the heat source. Usually, the pressure and temperature of the turbine inlet are optimized to have good cycle performance. The turbine inlet temperature may be lower than the heat source temperature. The heat source temperature actually is the heat carrier fluid temperature entering the evaporator. Then the pinch temperature difference analysis was performed to determine the mass flow rate and the outlet temperature of the heat carrier fluid. Because the mass flow rate and the outlet temperature of the heat carrier fluid are not specified initially, the thermal efficiency of the ORC has nothing to do with the turbine power output. Sometimes the thermal efficiency is high, but the turbine power output is low. Under such circumstance the outlet heat carrier fluid still has relatively "high" temperature, indicating the not full recovery of the waste heat.

From a practical application point of view, engineers are interested in what are the optimal running parameters for an ORC under the given mass flow rate, inlet and outlet temperatures of the heat carrier fluid of the waste heat source. The heat carrier fluid can be flue gas, water, etc. The objective of this paper is to present a new design strategy for ORCs, based on the similarity analysis of two triangles in the T (temperature)–Q (heating power) curve. With constraint of the heat source and pinch temperature difference, five cases were computed to identify the optimal running parameters. Effects of inlet and outlet heat carrier fluid temperatures and pinch temperature differences on the cycle performance were analyzed. The exergy destruction in various components of the ORC is discussed. The present design method directly relates the system thermal efficiency with the turbine power output.

2. The problem statement and its solution strategy

2.1. The problem statement

Fig. 1a shows an ORC coupling with a heat source. The heat source is characterized with a mass flow rate of m_{gas}, inlet temperature of $T_{gas,in}$, and outlet temperature of $T_{gas,out}$ for the heat carrier fluid. The heat carrier fluid can be flue gas, water, etc. Here we use flue gas as a representative fluid with its physical properties identical to dry air at atmospheric pressure. The flue gas transfers heat to the ORC by an evaporator. The organic fluid within the ORC has a saturated or superheated vapor state with a high pressure at the expander (or turbine) inlet (point 1 in Fig. 1a). Then the vapor expands in the expander to produce useful power to reach a superheated vapor state with a low pressure at the turbine outlet (point 2). The condenser cools the vapor to reach a saturated liquid state at the pump inlet (point 4). Then the organic fluid is pressurized by a pump to reach a high pressure at the pump outlet (point 5).

Fig. 1b shows the T–s graph for such a Rankine cycle. The organic fluid consecutively has a subcooled liquid state at point 5, a saturated liquid state at point 6, a saturated vapor state at point 7, and a superheated vapor state at point 1, due to the continuous heating by the heat carrier fluid in the evaporator. The process 1–2s is an ideal isentropic expansion. A real expansion process is an entropy increase one (the process 1–2 in Fig. 1b). Alternatively, the continuous cooling by the condenser yields the organic fluid to have a superheated vapor state at point 2, a saturated vapor state at point 3, and a saturated liquid state at point 4.

Neglecting pressure drops in the evaporator and condenser, there are two pressures in the ORC: a high pressure of $P_5 = P_6 = P_7 = P_1$, and a low pressure of $P_2 = P_3 = P_4$. The isothermal boiling in the evaporator yields $T_6 = T_7$, and the isothermal condensation in the condenser leads to $T_3 = T_4$. Usually, the organic fluid is cooled by air or water with environment temperature. Thus we assume $T_3 = T_4 = 303.15$ K (30 °C). The evaporation pressure is $P_5 = P_6 = P_7 = P_1 = P_{sat}(T_6) = P_{sat}(T_7)$, and the condensation pressure is $P_2 = P_3 = P_4 = P_{sat}(T_3)$.

The new design method is to identify the internal relationship of various running parameters for the ORC with constraint of given heat source and pinch temperature difference in the evaporator. Besides, engineers are interested in the optimal running parameters for the organic fluid. This is a preliminary study using the proposed design method for the ORC, thus the internal heat exchanger (IHE) is not included in such a cycle.

2.2. The solution strategy

Because m_{gas}, $T_{gas,in}$ and $T_{gas,out}$ are given, the total heat received by the evaporator (or the whole system) is

$$Q_a = m_{gas} C_{p,gas} (T_{gas,in} - T_{gas,out}) \quad (1)$$

where $C_{p,gas}$ is the average specific heat of the heat carrier fluid based on the temperature of $0.5(T_{gas,in} + T_{gas,out})$. Neglecting variations of the specific heat versus temperatures, the heat transfer process yields the linear curve of AB for the heat carrier fluid in Fig. 2. The line AB has the following equation:

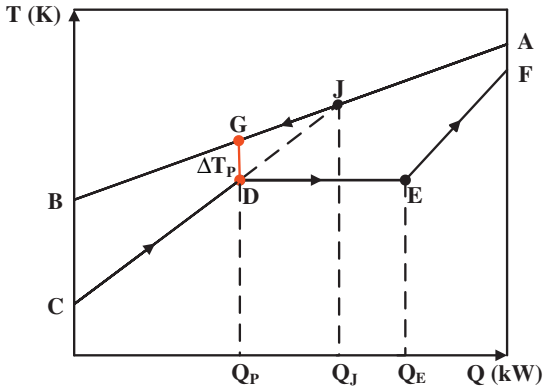

Fig. 2. Schematic T–Q curves for heat carrier fluid and organic fluid (A) (Q_a, $T_{gas,in}$), (B) (0, $T_{gas,out}$), (C) (0, $T_5 \approx T_4$), (D) (Q_P, T_6), (E) (Q_E, $T_7 = T_6$), (F) (Q_a, T_1), (G) (Q_P, $T_{p,gas}$), (J) (Q_J, $T_{J,gas}$).

$$Q = m_{gas} C_{p,gas} (T - T_{gas,out}) \tag{2}$$

The solution strategy consists of two major steps. The first step is to determine a suitable turbine inlet pressure for a given turbine inlet temperature, matching the heat source and pinch temperature difference constraints. The second step is to determine the optimal running parameters by analyzing the cycle performance versus a set of turbine inlet temperatures.

We record the turbine inlet temperature as T_1 (point F in Fig. 2). Because P_1 is not known at this stage, a P_1 is assumed at first. Then the organic fluid enthalpy at the turbine inlet is $h_1 = h_1(P_1, T_1)$. The mass flow rate of the organic fluid is decided by the following equation:

$$Q_a = m_{ORC}(h_1 - h_5) \tag{3}$$

By neglecting the enthalpy increase due to the pumping effect, we have $h_5 \approx h_4$, in which h_4 is the saturated liquid enthalpy at point 4 in Fig. 1.

The T–Q curve for the organic fluid is represented by the curve CD, DE, and EF (see Fig. 2). Points of C, D, E, and F correspond to points of 5, 6, 7, and 1, respectively in Fig. 1b. The equation for the CD part is written as

$$Q = m_{ORC} C_{p,f} (T - T_5) \approx m_{ORC} C_{p,f} (T - T_4) \tag{4}$$

where $C_{p,f}$ is the specific heat of the organic fluid (liquid). The line AB for the heat carrier fluid and the line CD for the organic fluid are crossed at the junction point J in Fig. 2. Coordinates at the point J can be determined by combining Eqs. (2) and (4). The pinch temperature difference (ΔT_P) across the two sides of the heat carrier fluid and the organic fluid is marked as GD in Fig. 2. Because the triangle GDJ is similarity to the triangle BCJ, i.e., $\Delta GDJ \sim \Delta BCJ$, we have

$$\frac{|GD|}{|BC|} = \frac{|JD|}{|JC|} = \frac{|JD|\cos\alpha}{|JC|\cos\alpha} \tag{5}$$

where α is the angle for the line CD with respect to the horizontal axis Q. Eq. (5) is further written as

$$\frac{\Delta T_P}{T_{gas,out} - T_5} \approx \frac{\Delta T_P}{T_{gas,out} - T_4} = \frac{Q_J - Q_P}{Q_J} \tag{6}$$

Eq. (6) decides Q_P at the point D because Q_J is already known. By substituting Q_P into Eq. (4), the vertical coordinate at the point D is known as the T_6. A new evaporation pressure of P_6 can be determined corresponding to its saturation temperature of T_6.

The length of DE is the latent heat of evaporation accounting for the mass flow rate of the organic fluid, which is expressed as

$$Q_E - Q_P = m_{ORC} h_{lg,ORC} \tag{7}$$

where $h_{lg,ORC}$ is the latent heat of evaporation for the organic fluid. Eq. (7) locates the point E.

We note that $P_1 = P_6$. The newly obtained turbine inlet pressure P_1^* may be different from the previous P_1. Thus the iterative procedure should be performed to repeat the above procedure, until P_1 is converged. We use the criterion of

$$|P_1 - P_1^*| < 10^{-6} \tag{8}$$

where P_1^* is the turbine inlet pressure at the current iteration step.

Note that 1–2s is an ideal isentropic process and 1–2 is an entropy increase process in the turbine (see Fig. 1b). The isentropic efficiency of the turbine is defined as:

$$\eta_{s,\exp} = \frac{h_1 - h_2}{h_1 - h_{2s}} \tag{9}$$

Now we decided all the state parameters in Figs. 1b and 2. The next step is to perform computations for a set of turbine inlet temperatures. Analyzing the cycle performance yields the optimal running parameters. Fig. 3 is the solution strategy illustrated by the block diagram, helping readers to easily understand the computation process.

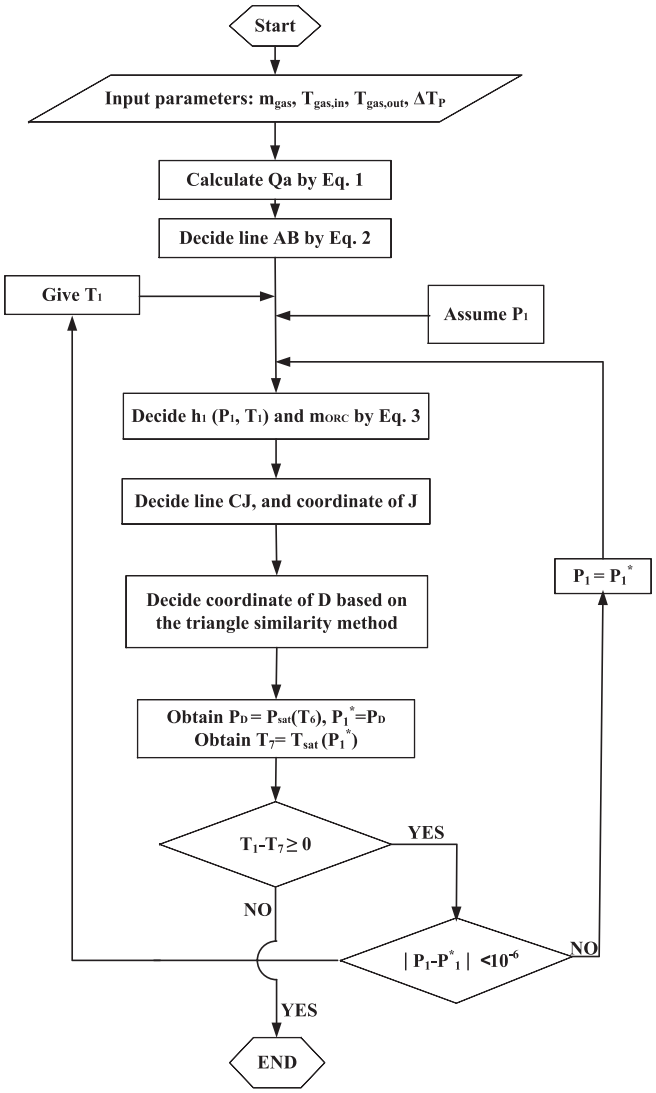

Fig. 3. The design strategy illustrated by the block diagram.

2.3. The cycle performance analysis

After all the state parameters in an ORC are determined, we compute the exergy destruction and exergy efficiency in various components of the ORC. The exergy destruction is defined as the inlet exergy subtracting the outlet exergy, and the exergy efficiency is defined as the used exergy divided by the available exergy. The reference state is the ambient atmosphere with the temperature and pressure of 293.15 K and 0.1 MPa respectively. Expressions of exergy destruction and efficiency for each component and the whole system are written as follows based on Mago et al. [38] and Tchanche et al. [39].

- for the evaporator

$$I_{ex,eva} = (E_{gas,in} + E_5) - (E_{gas,out} + E_1) \tag{10}$$

$$\eta_{ex,eva} = \frac{E_1 - E_5}{E_{gas,in} - E_{gas,out}} \tag{11}$$

where $E_{gas,in}$ and $E_{gas,out}$ are the inlet exergy and outlet exergy of the heat carrier fluid, E_1 and E_5 are the outlet exergy and inlet exergy of the organic fluid, respectively. $I_{ex,eva}$ and $\eta_{ex,eva}$ are the exergy destruction and exergy efficiency for the evaporator, respectively.

- for the turbine (expander)

The useful power output is

$$W_t = m_{ORC}(h_1 - h_2) \tag{12}$$

The exergy destruction and exergy efficiency are as follows

$$I_{ex,\exp} = E_1 - (E_2 + W_t) \tag{13}$$

$$\eta_{ex,\exp} = \frac{W_t}{E_1 - E_2} \tag{14}$$

- for the condenser

$$I_{ex,con} = (E_2 + E_{water,in}) - (E_4 + E_{water,out}) \tag{15}$$

$$\eta_{ex,con} = \frac{E_{water,out} - E_{water,in}}{E_2 - E_4} \tag{16}$$

where $E_{water,out} - E_{water,in}$ is the used exergy and E_2–E_4 is the available exergy for the condenser. The condenser was cooled by cooling water, with inlet and outlet temperatures of 2931.15 K and 298.15 K, respectively. The flow rate of cooling water was determined by the dissipated heat by the condenser.

- for the pump

The pumping power is

$$W_p = m_{ORC}(h_5 - h_4) \tag{17}$$

The isentropic efficiency of the pump is defined as

$$\eta_{s,p} = \frac{h_{5s} - h_4}{h_5 - h_4} \tag{18}$$

The exergy destruction and exergy efficiency are

$$I_{ex,p} = (W_p + E_4) - E_5 \tag{19}$$

$$\eta_{ex,p} = \frac{E_5 - E_4}{W_p} \tag{20}$$

- for the whole system

The thermal efficiency is

$$\eta_{ORC} = \frac{W_t - W_p}{Q_a} \tag{21}$$

The exergy destruction for the whole system is the sum of the exergy destruction for each component.

$$I_{ex,sys} = I_{ex,eva} + I_{ex,\exp} + I_{ex,con} + I_{ex,p} \tag{22}$$

The system exergy efficiency is

$$\eta_{ex,sys} = \frac{E_{sys,u}}{E_{sys,a}} \tag{23}$$

where $E_{sys,u}$ is the used exergy for the whole system and $E_{sys,a}$ is the available exergy of the system.

3. Results and discussion

3.1. Application of the present ORC design method

ORC is a hot research area in recent years due to the demand of recovering low grade heat. Articles in the open literature majorly focused on the discussion of the ORC itself, not coupling with the heat source. Based on the heat carrier fluid, the heat source can either be flue gas or water. There are large amount of flue gas waste heat in industries. Because water–vapor may be included in flue gas, waste heat recovery includes the sensible heat recovery and latent heat recovery. For the latent heat recovery, the exit flue gas temperature should be below the dew point so that latent heat of vapor in the flue gas can be extracted. Here we deal with the sensible heat recovery. In Beijing (China) about one-third of the heat supply in winter season was provided by natural gas boilers. The flue gas with its flow rate of about 17t/h (~4.7 kg/s) and temperature of 200–300 °C is directly discharged into environment by each natural gas boiler. Recovering the waste heat by ORC greatly attracts the heat supply company. In this paper we arrange five design cases based on the waste heat source of each natural gas boiler. The major design parameters are coming from this application background. We use the flue gas flow rate, inlet and outlet temperatures and pinch temperature difference as the input parameters. The solution strategy gives a complete set of output parameters such as the system thermal and exergy efficiencies, organic fluid mass flow rate, and running pressure. Because the total heat extracted from the heat source is fixed in the solution, the obtained thermal efficiency directly achieves the effective turbine power. Thus the economic performance by using ORC can be evaluated. In order to explore the maximum turbine power, we perform the sensitivity analysis of the flue gas exit temperature on the system performance. All these results are detailed described in the following sections.

3.2. Running cases

Table 1 shows the five design cases. Cases 1–3 are for the flue gas mass flow rate and inlet temperatures of 4.623 kg/s and 573.15 K (300 °C). Case 1 is for a fixed flue gas exit temperature of 363.15 K but case 2 is for a varied flue gas exit temperatures in the range of 348.15–383.15 K. The maximum turbine power can be searched by changing the flue gas exit temperature, which

Table 1
The five running cases computed in this paper.

Case	m_{gas} (kg/s)	$T_{gas,in}$ (K)	$T_{gas,out}$ (K)	Q_a (kW)	ΔT_p (K)
1	4.623	573.15	363.15	1000	5
2	4.623	573.15	348.15–383.15	905–1071	5
3	4.623	573.15	363.15	1000	15
4	6.131	523.15	363.15	1000	5
5	6.131	523.15	363.15	1000	15

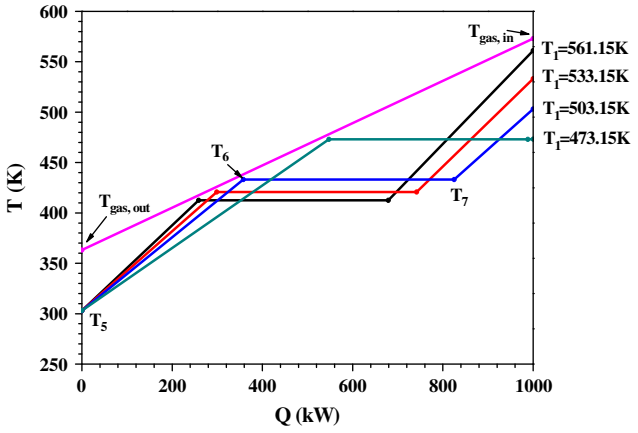

Fig. 4. The *T*–*Q* curves for four different turbine inlet temperatures with constraints of heat source and pinch temperature difference for case 1.

is a main objective of this paper. Both cases 1 and 2 had the same pinch temperature difference of 5 K. Case 3 had a pinch temperature difference of 15 K. Cases 4 and 5 are for a relatively lower inlet flue gas temperature of 523.15 K (250 °C). The pinch temperature difference is 5 K for case 4 and 15 K for case 5. For cases 1, 3, 4 and 5, the flue gas mass flow rate is arranged so that the recovery heat is Q_a = 1000 kW (1 MW). The case 2 has a varied recovery heat because the flue gas exit temperature is changed in a narrow range. Effect of pinch temperature differences on the cycle performance can be identified by comparing cases 1 and 3 for a higher inlet flue gas temperature of 573.15 K, and by comparing cases 4 and 5 for a lower inlet flue gas temperature of 523.15 K. Alternatively, effect of the inlet flue gas temperatures on the cycle performance can be identified by comparing cases 1 and 4 for the pinch temperature difference of 5 K, and by comparing cases 3 and 5 for the pinch temperature difference of 15 K. It is noted that the isentropic efficiencies for the turbine and pump are set to be 0.85.

Many organic working fluids are evaluated in the literature. However, the objective of this study is to present a new design method for ORCs coupling with the heat source. Thus only one organic working fluid, i.e., benzene is used here. Benzene is suitable for high temperature heat sources and is a dry fluid. The critical temperature and pressure are T_c = 562.05 K and P_c = 4.894 MPa, respectively. Because the critical temperature is high and approaches the inlet flue gas temperature, the ORC should be operating at subcritical pressure. Besides, benzene is a slightly-poisonous fluid and has a high auto-ignition temperature for its safe operation. The physical properties of benzene are computed by the widely used NIST software.

3.3. Basic cycle performance by the design method

Fig. 4 shows the *T*–*Q* curve for case 1. Because the problem uses the turbine inlet temperature (T_1) as the independent parameter, the determination of the *T*–*Q* curves should satisfy the constraint of heat source and pinch temperature difference. Four curves for the organic fluid side are given in Fig. 4, corresponding to four different T_1 of 561.15 K, 533.15 K, 503.15 K and 473.15 K, respectively. The iterative procedure described in Section 2.2 shows that the iterative process is not converged for the turbine inlet temperatures smaller than 473.15 K, indicating that 473.15 K is almost the minimum temperature that can satisfy the heat source and pinch temperature difference constraints. As noted previously, the organic fluid may have the states of subcooled liquid, saturated liquid, saturated vapor, and superheated vapor, respectively. For each T_1, the *T*–*Q* curve has a horizontal line section indicating the isothermal boiling. Among the four T_1 values presented, the maximum turbine inlet temperature of 561.15 K requires a minimum saturation temperature of $T_6 = T_7$ = 412.46 K, corresponding to a minimum turbine inlet pressure of $P_1 = P_{sat}(T_6)$ = 0.466 MPa. On the other hand, the minimum turbine inlet temperature of 473.15 K refers to a maximum saturation temperature of $T_6 = T_7$ = 469.36 K, corresponding to the maximum turbine inlet pressure of 1.353 MPa. It is also found that there is a very small

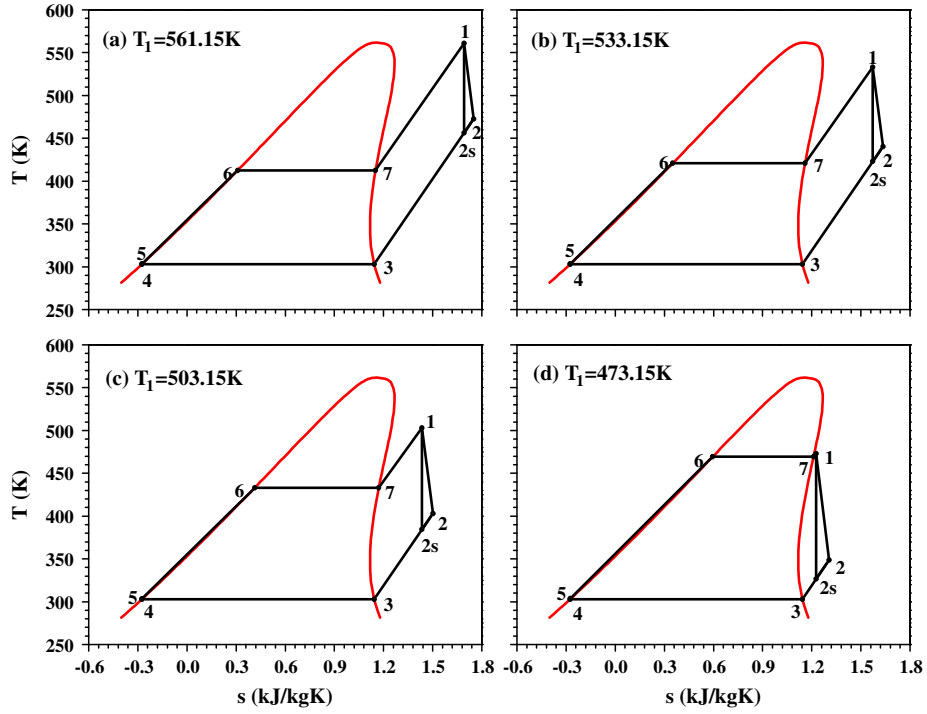

Fig. 5. The *T*–*s* diagram with four different turbine inlet temperatures for case 1.

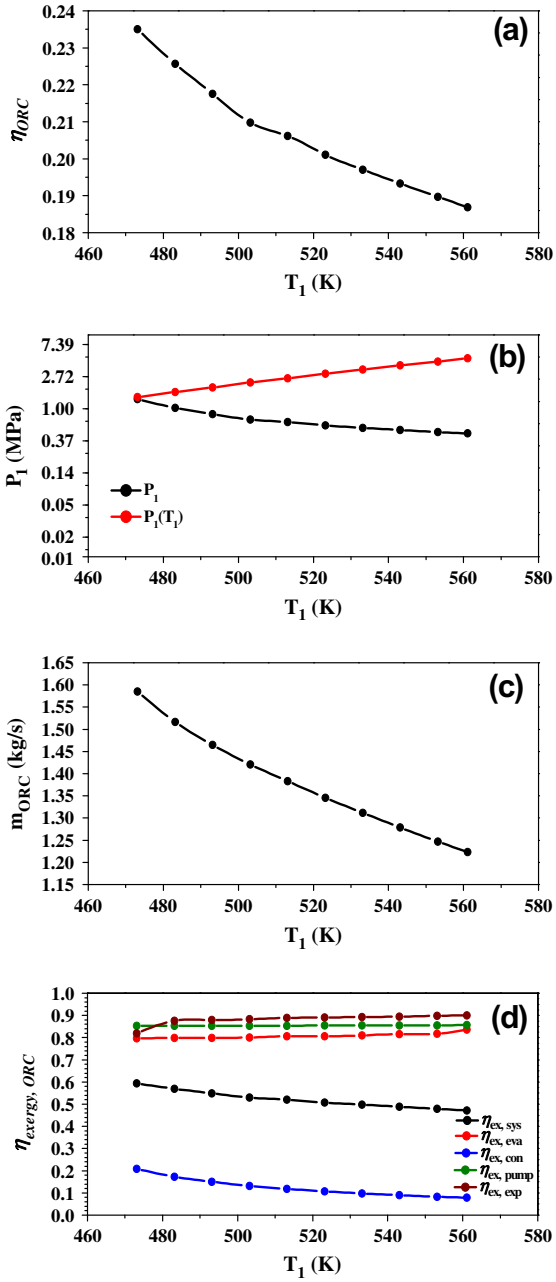

Fig. 6. The cycle performance versus the turbine inlet temperatures for case 1.

Table 2
The inlet and outlet exergy, exergy destruction, used and available exergy for component and system (case 1, T_1 = 561.15 K).

Element	$E_{i,in}$ (kW)	$E_{i,out}$ (kW)	I_i (kW)	$E_{i,u}$ (kW)	$E_{i,a}$ (kW)	$\eta_{ex,i}$ (%)
Pump	0.98	0.87	0.11	0.64	0.75	85.4
Evaporator	396.80	330.11	66.30	295.53	362.94	81.6
Turbine	296.40	275.49	20.91	187.62	208.53	89.9
Condenser	87.87	7.09	80.78	6.86	80.71	7.8
Total system	396.91	222.19	174.72	186.87	393.94	47.2

superheated vapor flow section in the evaporator for the lowest T_1 of 473.15 K.

Fig. 5 shows the *T–s* diagrams with the four turbine inlet temperatures for case 1. The saturation temperatures (points 6–7)

Table 3
The inlet and outlet exergy, exergy destruction, used and available exergy for component and system (case 1, T_1 = 473.15 K).

Element	$E_{i,in}$ (kW)	$E_{i,out}$ (kW)	I_i (kW)	$E_{i,u}$ (kW)	$E_{i,a}$ (kW)	$\eta_{ex,i}$ (%)
Pump	3.17	2.75	0.42	2.46	2.87	85.4
Evaporator	398.68	339.27	59.41	302.86	362.94	83.6
Turbine	192.79	169.79	22.99	237.94	274.39	86.7
Condenser	31.22	6.75	24.47	6.45	30.92	20.9
Total system	397.81	278.10	119.71	235.07	393.94	59.3

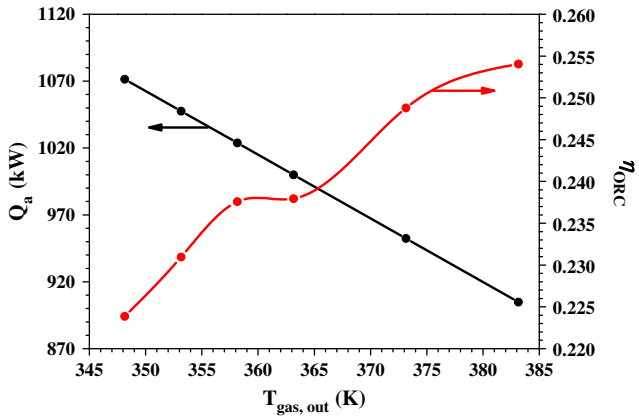

Fig. 7. The heat received by the ORC versus the flue gas exit temperatures (case 2).

are increased with continuous decreases in the turbine inlet temperatures (T_1). Point 1 (turbine inlet state) is gradually approaching the red[1] curve envelope, and it is on the red curve margin for T_1 = 473.15 K (see Fig. 5d). Point 1 is far away from the red curve envelope for high turbine inlet temperature, thus the entropy increase in the evaporator is also large for high T_1 values. Because benzene is a dry fluid, point 2 is always in the vapor state. The temperature increase by the pumping effect is very small, thus points 4 and 5 almost coincide with each other for all of the four *T–s* diagrams.

We identify the cycle performance in Fig. 6 for case 1. The system thermal efficiency (η_{ORC}), turbine inlet pressure (P_1) and mass flow rate (m_{ORC}) are decreased with increases in the turbine inlet temperatures (see Fig. 6a–c). The decreased thermal efficiency at high turbine inlet temperature is due to the fact that a high turbine inlet temperature requires a low turbine inlet pressure to satisfy the constraints of heat source and pinch temperature difference in evaporators. A saturated vapor state at point 1 has the optimal (maximum) thermal efficiency, which is 23.51% at T_1 = 473.15 K. Fig. 6b shows that the turbine inlet pressure P_1 is decreased with increases in T_1. But the difference between P_{sat} (T_1) and P_1 is increased with increases in T_1, indicating the increased superheating degree of the vapor at the turbine inlet with increases in T_1. The decreased mass flow rate of the organic fluid with increases in T_1 is due to the large enthalpy at high T_1. The pressure has mini influence on the enthalpy in the vapor state. Thus a smaller mass flow rate of the organic fluid is required to receive a given heat from the flue gas at high T_1 values.

Tables 2 and 3 show the exergy destruction, used and available exergy for the component and system, which are given for case 1 with turbine inlet temperatures of 561.15 K (Table 2) and

[1] For interpretation of color in Figs. 1, 2, 4–7 and 9–14, the reader is referred to the web version of this article.

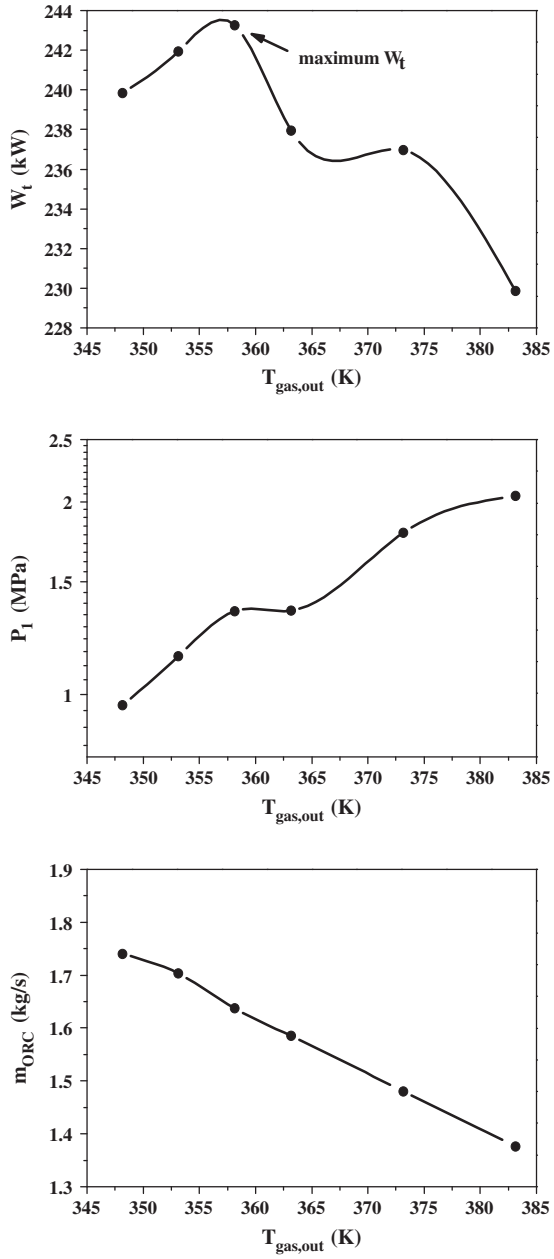

Fig. 8. The effective turbine power, turbine inlet pressure and mass flow rate of the organic fluid versus flue gas exit temperatures (case 2).

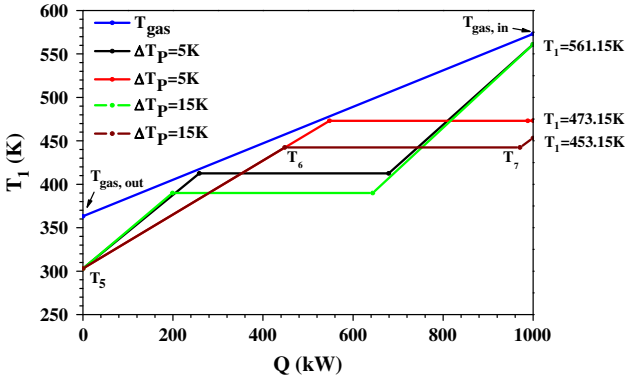

Fig. 9. Effect of pinch temperature differences on the *T*–*Q* curves for the organic fluid: a comparison between cases 1 and 3.

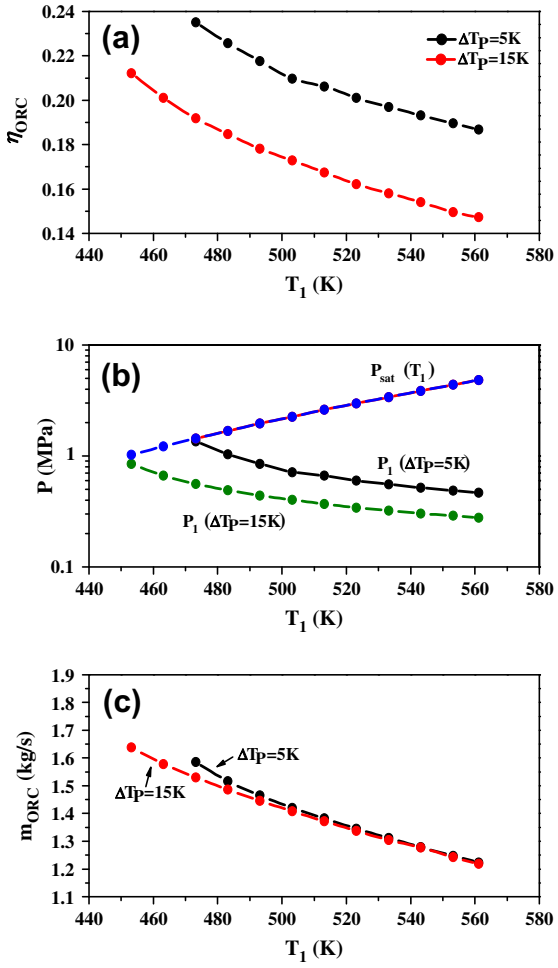

Fig. 10. Effect of pinch temperature differences on the cycle performance: a comparison between cases 1 and 3.

473.15 K (Table 3). The lower T_1 condition approaches the optimal running state. The pump, evaporator and turbine have higher exergy efficiencies than the condenser (see Tables 2 and 3). The condenser exergy efficiency is 20.9% at T_1 = 473.15 K, and it is increased with decreases in the condenser inlet temperatures.

The condenser exergy efficiencies are lower than those reported by Mago et al. [38]. This is because benzene has significantly different physical properties with R113 studied by Mago et al. [38]. For instance, the present study gave T_2 = 348.68 K (condenser inlet temperature) and e = 19.694 kJ/kg (inlet exergy per unit mass flow rate), corresponding to the available exergy of 19.506 kJ/kg at T_1 = 473.15 K for benzene. Mago et al. [38] gave the condenser inlet temperature of 340.83 K and exergy of 3.673 kJ/kg for R113, the available exergy was 3.673 kJ/kg (see Table V in Mago et al. [38]). Compared with R113 [38], benzene has much larger available exergy across the condenser inlet and outlet to reach lower condenser exergy efficiencies.

The higher system exergy efficiency is also attributed to the different working fluids used in this study and in Mago et al. [38]. Both studies calculated the ORCs with the heat source temperatures of 573.15 K. Benzene has the critical pressure and temperature of 4.894 MPa and 562.05 K respectively. Thus it is suitable for the high heat source temperature applications such as encountered in this study. Thus better evaporator and turbine performances are achieved due to the two components working in the high temperature region, leading to higher system exergy efficiency. However, R113 has the critical pressure and temperature

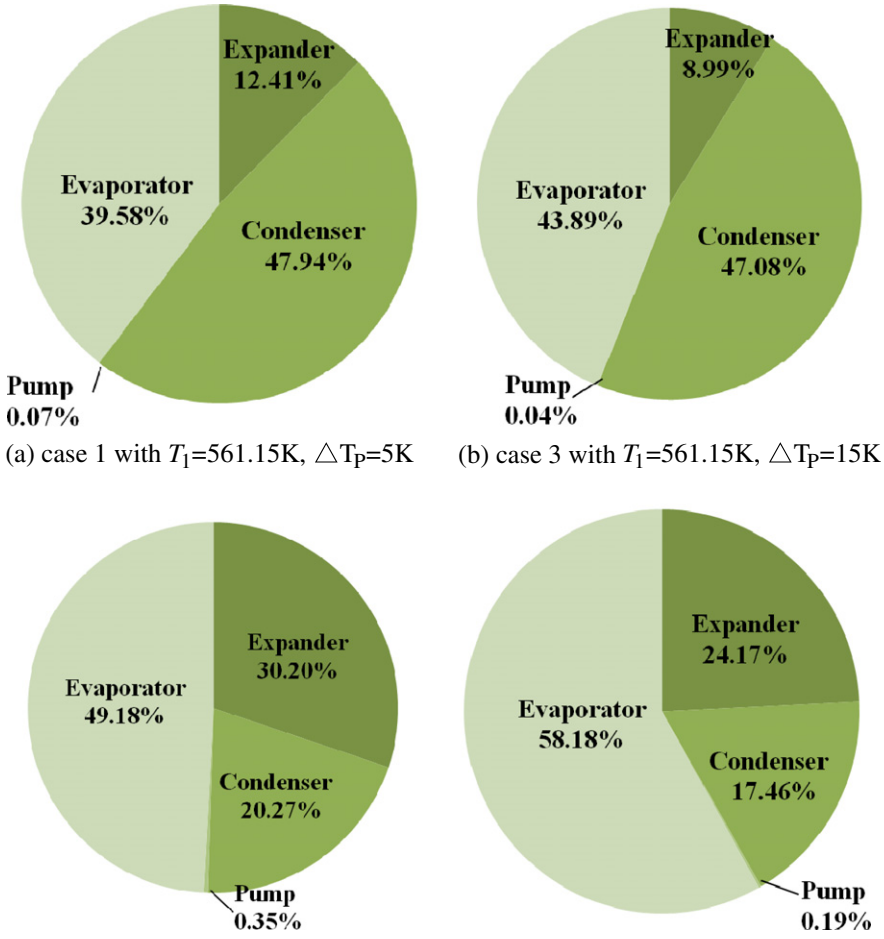

(a) case 1 with T_1=561.15K, △T_P=5K (b) case 3 with T_1=561.15K, △T_P=15K

(c) case 1 with T_1=473.15K, △T_P=5K (d) case 3 with T_1=453.15K, △T_P=15K

Fig. 11. Exergy destruction contributed by each component of the ORC: effect of turbine inlet temperatures and pinch temperature differences.

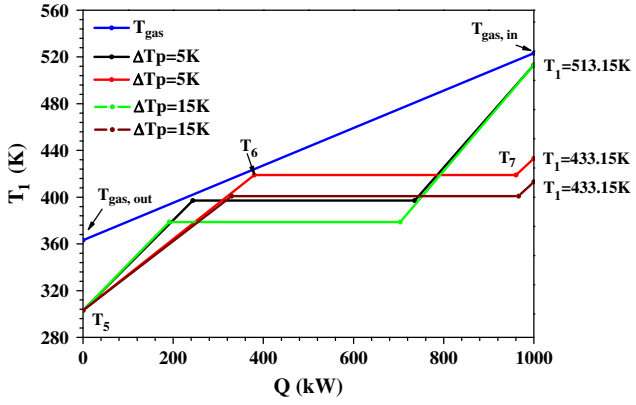

Fig. 12. Effect of pinch temperature differences on the *T*–*Q* curve: a comparison between cases 4 and 5.

of 3.392 MPa and 487.21 K, which is suitable for the medium or low heat source temperature applications (<473 K). When R113 was used with the heat source temperature of 573.15 K [38], it yields the lower exergy efficiencies of the evaporator and turbine due to the two components working in the high temperature region. But the condenser exergy efficiency is higher because the condenser is running under low temperature condition.

Fig. 6c further shows component and system exergy efficiencies. The exergy efficiencies of evaporator, pump and expander do not change significantly versus turbine inlet temperatures. The system exergy efficiency is 59.3% at T_1 = 473.15 K and 47.2% at T_1 = 561.15 K.

3.4. The maximum turbine power

The above analysis fixes an arbitrary flue gas exit temperature of 363.15 K (90 °C). The question may arise on what is the suitable flue gas exit temperature to achieve the maximum turbine power. We perform the sensitivity analysis of the flue gas exit temperatures on the system performance. Fig. 7 shows the decreased heat extracted from the flue gas with increases in the flue gas exit temperatures at the mass flow rate of 4.623 kg/s and inlet temperature of 573.15 K (see case 2 in Table 1). The system thermal efficiencies are increased with increases in the flue gas exit temperatures (see Fig. 7).

Fig. 8 identifies the turbine power, turbine inlet pressure and mass flow rate of the organic fluid against the flue gas exit temperatures. It is interesting to note that the turbine power has a parabola distribution versus the flue gas exit temperatures. With increases in the flue gas exit temperatures, the turbine powers are increased, achieve the maximum value at $T_{gas,out}$ = 358.15 K, and then decreased. The turbine inlet pressures are increased and mass flow rates of the organic fluid are decreased with increases in the flue gas exit temperatures. At the turbine inlet pressure of 1.348 MPa, mass flow of the organic fluid of 1.637 kg/s, the turbine power attains the maximum value of 243 kW. Considering the

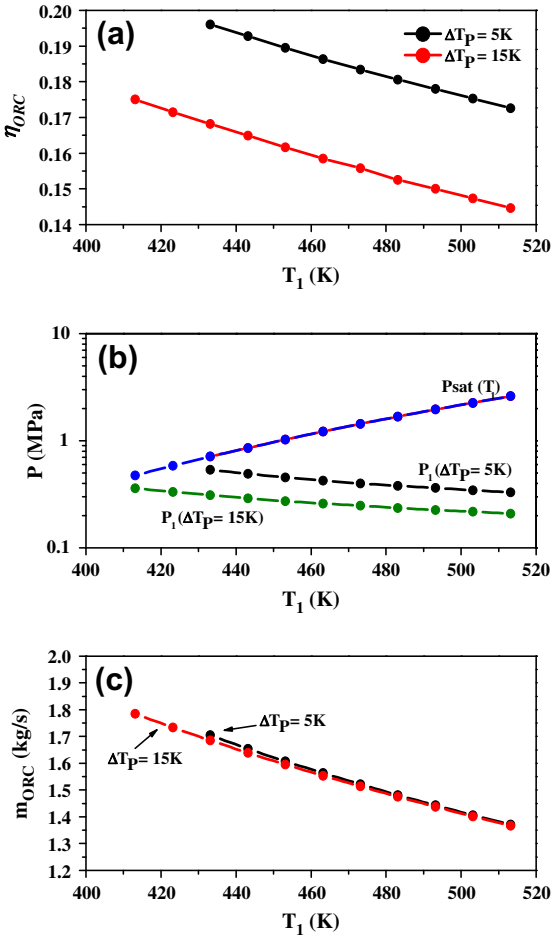

Fig. 13. Effect of pinch temperature differences on the cycle performance: a comparison between cases 4 and 5.

design parameter of flue gas flow rate of 17t/h and temperature of 573.15 K emitted by each natural gas boiler of Beijing Heat Supply Company, the ORC technology can create 243 kW electricity with the flue gas exit temperature of 358.15 K. Assuming the 6 months operation for each year, the company can generate the electricity of 1 million KWh and reduce the carbon dioxide emission by 997t annually. Giving the ORC price by 10,000 RMB/kW, the company can recoup the investment cost by about 2.5 years.

3.5. Effect of pinch temperature differences on the cycle performance

Fig. 9 shows the T–Q curves for two pinch temperature differences of 5 K and 15 K (see cases 1 and 3 in Table 1). The heat source is the same for the two cases. The major finding is the decreased isothermal boiling temperature with increases in the pinch temperature differences. For example, for the 1 MW heat received from the flue gas, the saturation temperature of T_6 ($T_7 = T_6$) is decreased from 412.46 K for $\Delta T_p = 5$ K to 389.95 K for $\Delta T_p = 15$ K, at $T_1 = 561.15$ K. Correspondingly, the turbine inlet pressure P_1 is decreased from 0.466 MPa for $\Delta T_p = 5$ K to 0.278 MPa for $\Delta T_p = 15$ K, causing the decreased thermal efficiency with increases in the pinch temperature differences. The optimal and maximum thermal efficiency is being approached when the turbine inlet temperatures are decreased, which appears at $T_1 = 473.15$ K for $\Delta T_p = 5$ K, and $T_1 = 453.15$ K for $\Delta T_p = 15$ K. The pinch temperature differences of 5 K and 15 K yield slightly-superheated vapor states at the turbine inlet, respectively. The isothermal boiling temperatures in the two-phase region are $T_6 = T_7 = 469.36$ K for $\Delta T_p = 5$ K and $T_6 = T_7 = 442.31$ K for $\Delta T_p = 15$ K, respectively.

Fig. 10 gives the effect of pinch temperature differences on the cycle performance. The system thermal efficiency (η_{ORC}) and turbine inlet pressure (P_1) are decreased with increases in the turbine inlet temperatures. They are also decreased with increases in the pinch temperature differences. The maximum thermal efficiency is 23.51% for $\Delta T_p = 5$ K, and 21.64% for $\Delta T_p = 15$ K (see Fig. 10a). The deference between the saturation pressure corresponding to T_1 and the turbine inlet pressure P_1 is increased with increases in the pinch temperature differences (see Fig. 10b), indicating the increased vapor superheating degree at the turbine inlet for high pinch temperature differences. The pinch temperature differences have small influence on the mass flow rate of the organic fluid (see Fig. 10c), due to the weakly dependent of the vapor enthalpy on pressure at the turbine inlet. The increased pinch temperature differences can slightly enlarge the operation range of turbine inlet temperatures.

The exergy destruction in various components was examined in Fig. 11 using the biscuit diagram. At high turbine inlet temperatures of $T_1 = 561.15$ K, the condenser contributes the major exergy destruction. The evaporator and expander are the second and third contributors of the exergy destruction (see Fig. 11a and b). Increase of the pinch temperature differences slightly increases the exergy destruction contribution for the evaporator, but decreases the exergy destruction contribution for the expander (see Fig. 11a and b). The large exergy destruction contribution by the condenser is due to the enlarged superheating vapor flow section for high turbine inlet temperatures. When the turbine inlet temperature is reduced to the optimal condition, the evaporator contributes the major exergy destruction. The expander and condenser become the second and third contributors of the exergy destruction (see Fig. 11c and d). In other words, the condenser has the smallest exergy destruction except the pump, caused by the significantly decreased inlet temperature and shortened vapor superheating flow section in the condenser.

3.6. Discussion of a lower flue gas temperature case

A lower flue gas inlet temperature of 523.15 K (250 °C) was studied for case 4 with $\Delta T_p = 5$ K and case 5 with $\Delta T_p = 15$ K (see Table 1). The findings are summarized as follows:

1. The optimal (maximum) thermal efficiency appears at the small vapor overheating degree at the turbine inlet (see Fig. 12).
2. The system thermal efficiency, turbine inlet pressure and mass flow rate of the organic fluid are decreased with increases in the turbine inlet temperatures (see Fig. 13).
3. The high pinch temperature difference lowers the saturation temperature and pressure in the evaporator, decreasing the system thermal efficiency.
4. The mass flow rate of the organic fluid is insensitive to the pinch temperature differences.

The effect of the flue gas inlet temperatures on the cycle performance can be identified by comparing Figs. 12–14 with Figs. 9–11. The decreased flue gas inlet temperature reduces the turbine inlet temperature at the optimal condition. For instance, T_1 is 473.15 K (optimal condition) for $T_{gas,in} = 573.15$ K (see Fig. 9), but T_1 is decreased to 433.15 K for $T_{gas,in} = 523.15$ K for $\Delta T_p = 5$ K (see Fig. 12). The maximum system thermal efficiency is decreased from 23.51% for $T_{gas,in} = 573.15$ K to 19.61% for $T_{gas,in} = 523.15$ K (see Figs. 10a and 13a). The turbine inlet pressures are decreased with decreases in the flue gas inlet temperatures (see Figs. 10b and 13b). Because the received waste heat is the same for ($Q_a =$ 1 MW), an increased mass flow rate of the organic fluid is required for a lower flue gas inlet temperature (see Figs. 10c and 13c).

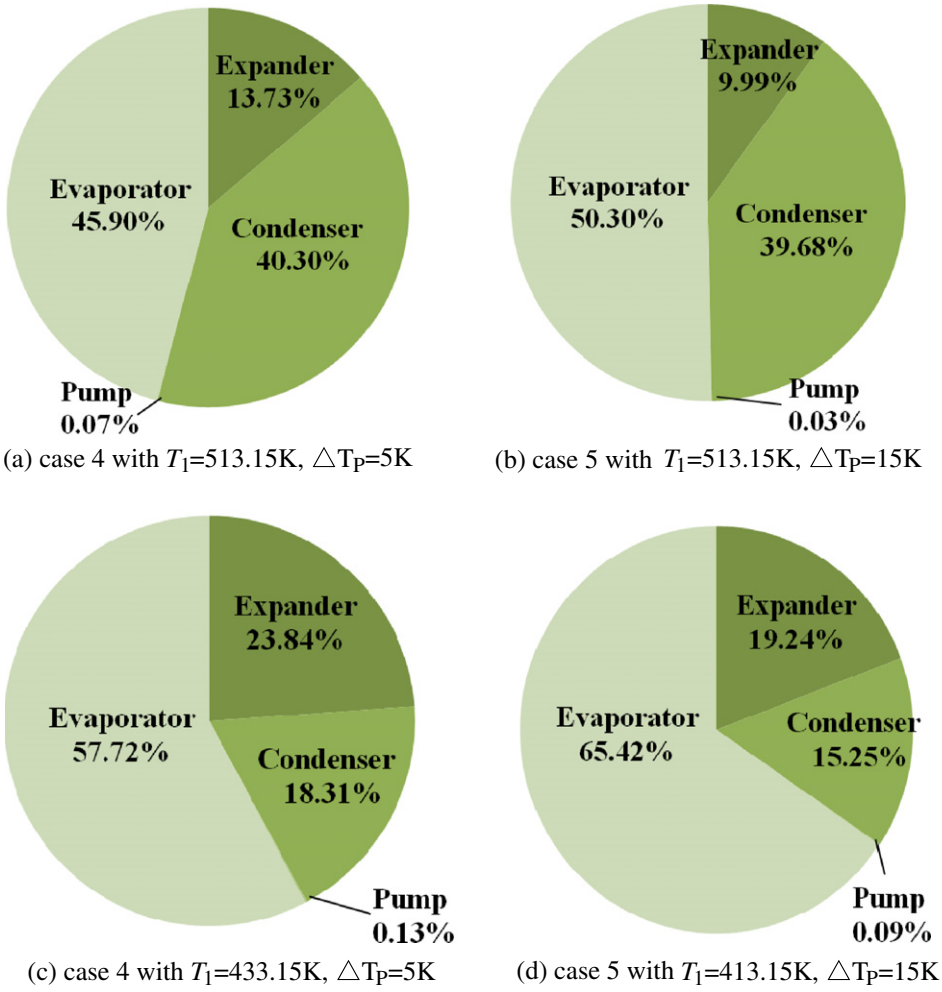

(a) case 4 with T_1=513.15K, △T_P=5K

(b) case 5 with T_1=513.15K, △T_P=15K

(c) case 4 with T_1=433.15K, △T_P=5K

(d) case 5 with T_1=413.15K, △T_P=15K

Fig. 14. Exergy destruction contributed by each component of the ORC: effect of turbine inlet temperatures and pinch temperature differences.

The changed flue gas inlet temperatures change the exergy destruction by each component of ORC. At high flue gas inlet temperature of 573.15 K, the condenser gave the maximum exergy contribution at the high turbine inlet temperature (see Fig. 11). But the maximum exergy destruction contributor switches to the evaporator for the lower flue gas inlet temperature (see Fig. 14). At the optimal condition at the reduced turbine inlet temperatures, the exergy destruction distributions by each component are similar for both high and low flue gas inlet temperatures, but the detailed values are slightly different (see Figs. 11c, d and 14c, d).

3.7. Comment on the new design method for ORC

Previous studies on ORC focus on the thermodynamic analysis with the cycle alone. After all the state parameters are determined, a suitable heat source is searched to match the pinch temperature difference in the evaporator, inducing the system thermal efficiency having no relationship with the turbine power. Under many situations, a waste heat source is characterized by a given heat source temperature and mass flow rate. Engineers strongly expect to decrease the flue gas exit temperature as low as possible, thus a desired recovery degree of the waste heat is reached to convert more thermal energy into useful power. The design method guides engineers to design a thermal power plant driven by the waste heat with the discharged flue gas temperature as low as possible. Besides, the method directly relates the system thermal efficiency with the useful turbine power. The higher the system thermal efficiency, the larger the useful power output is.

Holding the design method, the heat transfer design should be continued to reach a full design of the heat exchangers. The method gives a complete set of boundary conditions for the heat transfer analysis. For example, after the solution convergence is reached, all the parameters are determined, including the inlet and outlet temperatures, mass flow rate, and pressure for the organic fluid in the evaporator, ensuring very convenient heat transfer design for the evaporator. Besides, the thermodynamic analysis here specifies the parameter requirement for the selection of the turbine (or expander) machine, to attain an optimal condition.

The design method also provides a simple, but effective control strategy for ORCs. After the whole ORC system is finalized, the temperature and pressure at the turbine inlet, and mass flow rate of the organic fluid should be consistent with each other. In other words, the three parameters of T_1, P_1 and m_{ORC} are not independent parameters. A simple control strategy is to monitor and control the turbine inlet temperatures. Other parameters automatically adapt the change of the turbine inlet temperatures, to approach the optimal running condition, by neglecting the small parameter variations induced by the cooling capability of the environment water or air.

Because there is an isothermal boiling section in the evaporator for a subcritical pressure cycle, leading to the poor match between the heat carrier fluid and the organic fluid. The design method will be extended for the analysis of the supercritical Rankine cycle, or the cycle with binary working fluids. Under such circumstances, there is no isothermal boiling section. The temperatures of the organic fluid are continuously increased by adding more heat.

4. Conclusions

A design method for the thermodynamic analysis for ORCs was newly proposed, directly relating the turbine power with the system thermal efficiency and ensuring engineers to recover the waste heat with its flue gas exit temperature as low as possible. Benzene is used as the working fluid for the computations of five cases. With constraint of the given heat source and pinch temperature difference, the system thermal efficiency, turbine inlet pressure and mass flow rate of the organic fluid are decreased with increases in the turbine inlet temperatures. The optimal condition appears at the saturated or slightly-superheated vapor state at the turbine inlet. The increase in the pinch temperature differences yields the decreased turbine inlet pressure to reduce the system thermal efficiency. The pinch temperature differences do not have significant influence on the mass flow rate of the organic fluid. At higher turbine inlet temperatures, either the condenser or the evaporator contributes the major exergy destruction, depending on the flue gas inlet temperatures. At lower turbine inlet temperatures, the evaporator, expander and condenser are the first, second and third contributors of the exergy destruction to the whole system. The exergy destruction by the condenser is significantly decreased with decreases in the turbine inlet temperatures. Future work on the design method will be focused on the analysis of the supercritical Rankine cycle or the cycle with binary working fluids, under which there is no isothermal boiling section in the evaporator.

Acknowledgements

This work was supported by the national basic Research Program of China (2011CB710703), the natural science foundation of China (50825603 and 51106050), the Suzhou industry Project (SYG201105) and the Beijing Science and Technology Program (Z111109055311097).

References

[1] Utlu Z, Hepbasli A. A review on analyzing and evaluating the energy utilization efficiency of countries. Renew Sustain Energy Rev 2007;11:1–29.
[2] Lund PD. Effects of energy policies on industry expansion in renewable energy. Renewable Energy 2009;34:53–64.
[3] Resch G, Held A, et al. Potentials and prospects for renewable energies at global scale. Energy Policy 2008;36:4048–56.
[4] Klevas V, Streimikiene D, Kleviene A. Sustainability assessment of the energy projects implementation in regional scale. Renew Energy Rev 2009;13:155–66.
[5] Roy P, Desilets M. Thermodynamic analysis of a power cycle using a low-temperature source and a binary NH_3–H_2O mixture as working fluid. Int J Therm Sci 2010;49:48–58.
[6] Larjola J. Electricity from industrial wast heat using high-speed organic rankine cycle (ORC). Int J Prod Econ 1995;41:227–35.
[7] Hung TC, Shai TY, Wang SK. A review of organic rankine cycles (ORCs), for the recovery of low-grade waste heat. Energy 1996;22:661–7.
[8] Wei D, Lu U, Lu Z, Gu J. Dynamic modeling and simulation of an organic rankine cycle (ORC) system for waste heat recovery. Appl Therm Eng 2008;28:1216–24.
[9] Bianchi M, Pascale AD. Parametric investigation of available and innovative solutions for the exploitation of low and medium temperature heat sources. Appl Energy 2011;88:1500–9.
[10] Ammare Y, Joyce S. Low grade thermal energy sources and uses from the process industry in the UK. Appl Energy 2012;89:3–20.
[11] Zhu J, Zhang W. Optimization design of plate heat exchangers (PHEs) for geothermal district heating systems. Geothermics 2004;33:337–47.
[12] Douglas TC, Gregory SJ. Optimization of cross flow heat exchangers for thermoelectric waste heat recovery. Energy Convers Manage 2004;45:1565–82.
[13] Lin S, Luo X. Synthesis of multipass heat exchanger networks based on pinch technology. Comput Chem Eng 2011;35:1257–64.
[14] Bahaa S, Koglbauer G, Wendland M, Fisher J. Working fluids for low-temperature organic rankine cycles. Energy 2007;32:1210–21.
[15] Lakew AA, Bolland O. Working fluids for low-temperature heat source. Appl Therm Eng 2010;30:1262–8.
[16] Lai NA, Wendland M, Fischer J. Working fluids for high-temperature organic rankine cycles. Energy 2011;36:199–211.
[17] Liu B, Chien K, Wang C. Effect of working fluids on organic rankine cycle for waste heat recovery. Energy 2004;29:1207–17.
[18] Guo T, Wang HX, Zhang SJ. Selection of working fluids for a novel low-temperature geothermally-powered ORC based cogeneration system. Energy Convers Manage 2011;52:2384–91.
[19] Maizza V, Maizza A. Unconventional working fluids in organic rankine-cycles for waste energy recovery systems. Appl Therm Eng 2001;21:381–90.
[20] Hung T. Waste heat recovery of organic rankine cycle using dry fluids. Energy Convers Manage 2001;42:539–53.
[21] Chen Y, Lundqvist P, Johansson A, Platell P. A comparative study of the carbon dioxide transcritical power cycle compared with an organic cycle with R123 as working fluid in waste heat recovery. Appl Therm Eng 2006;26:2142–7.
[22] Roy JP, Mishra MK, Misra A. Performance analysis of an organic rankine cycle with superheating under different heat source temperature conditions. Appl Energy 2011;88:2995–3004.
[23] Wang JL, Zhao L, Wang XD. An experimental study on the recuperative low temperature solar rankine cycle using R245fa. Appl Energy 2012;94:34–40.
[24] Zhang S, Wang H, Guo T. Performance comparison and parametric optimization of subcritical organic rankine cycle (ORC) and transcritical power cycle system for low-temperature geothermal power generation. Appl Energy 2011;88:2740–54.
[25] Zhang XR, Yamaguchi H, Uneno D, Fujima K, Enomoto M, Sawada N. Analysis of a novel solar energy-powered rankine cycle for combined power and heat generation using supercritical carbon dioxide. Renewable Energy 2006;31:1839–954.
[26] Karellas S, Schuster A. Supercritical fluid parameters in organic rankine cycle applications. Int J Thermodyn 2008;11:101–8.
[27] Wang XD, Zhao L. Analysis of zeotropic mixtures used in low-temperature solar rankine cycles for power generation. Solar Energy 2009;83:605–13.
[28] Angelino G, Pallano PCD. Multicomponent working fluids for organic rankine cycles (ORCs). Energy 1998;23:449–63.
[29] Arima H, Okamoto A, Ikegami Y. Local boiling heat transfer characteristics of ammonia/water binary mixture in a vertical plate evaporator. Int J Refrig 2011;34:648–57.
[30] Chen H, Gowami DY. A supercritical rankine cycle using zeotropic mixture working fluids for the conversion of low-temperature heat into power. Energy 2011;36:549–55.
[31] Wang JL, Zhao L, Wang XD. A comparative study of pure and zeotropic mixtures in low-temperature solar rankine cycle. Appl Energy 2010;87:3366–73.
[32] Yamamoto T, Furuhata T. Design and testing of the organic rankine cycle. Energy 2001;26:239–51.
[33] Sun J, Li W. Operation optimization of an organic rankine cycle (ORC) heat recovery power plant. Appl Therm Eng 2011;31:2023–41.
[34] Dai Y, Wang J, Gao L. Parametric optimization and comparative study of organic rankine cycle (ORC) for low grade waste heat recovery. Energy Convers Manage 2009;50:576–82.
[35] Wei D, Lu H, Lu Z, Gu J. Performance analysis and optimization of organic rankine cycle (ORC) for waste heat recovery. Energy Convers Manage 2007;48:1113–9.
[36] Quoilin S, Aumann R, Grill A, Schuter A. Dynamic modeling and optimal control strategy of waste heat recovery organic rankine cycles. Appl Energy 2011;88:2183–90.
[37] Li J, Pei G, Ji J. Optimization of low temperature solar thermal electric generation with organic rankine cycle in different areas. Appl Energy 2010;87:3355–65.
[38] Mago PJ, Srinivasan KK, Chamra LM, Somayaji C. An examination of exergy destruction in organic rankine cycles. Int J Energy Res 2008;32:926–38.
[39] Tchanche BF, Lambrinos Gr, et al. Exergy analysis of micro-organic rankine power cycles for a small scale solar driven reverse osmosis desalination system. Appl Energy 2010;87:1295–306.